

Article

Analysis of the Mutual Impedance of Coils Immersed in Water

Peizhou Liu ^{*}, Tiande Gao [†] and Zhaoyong Mao [†]

School of Marine Science and Technology, Northwestern Polytechnical University, Xi'an 710072, China; gaotiande@nwpu.edu.cn (T.G.); maozhaoyong@nwpu.edu.cn (Z.M.)

* Correspondence: peizhou58@163.com; Tel.: +86-029-8848-5390

† These authors contributed equally to this work.

Abstract: Magnetic induction communication and wireless power transmission based on magnetic coupling have significant application prospects in underwater environments. Mutual impedance is a key parameter particularly required for the design of the systems. However, mutual impedance is usually extracted from measurements when the coils are processed, which is obviously not conducive to the system optimization in the design phase. In this paper, a model of the mutual impedance of coils immersed in water is established. The magnetic vector potential is expressed in the form of series by artificially setting a boundary, and then the mutual impedance calculation formula of the coils immersed in water is derived. In the analysis, the effect of the conductivity of water, the excitation frequency, and the number of turns of the coils are mainly taken into account. In addition, the variation of the mutual impedance of coils in air and water with axial displacement is also compared. The models can be used to analyze the coil coupling characteristics in the presence of conductive medium, which is helpful for the design process.

Keywords: mutual impedance; inductive power transfer; coils; water



Citation: Liu, P.; Gao, T.; Mao, Z. Analysis of the Mutual Impedance of Coils Immersed in Water. *Magnetochemistry* **2021**, *7*, 113. <https://doi.org/10.3390/magnetochemistry7080113>

Academic Editors: Panbo Liu and Roberto Zivieri

Received: 30 May 2021
Accepted: 3 August 2021
Published: 5 August 2021

Publisher's Note: MDPI stays neutral with regard to jurisdictional claims in published maps and institutional affiliations.



Copyright: © 2021 by the authors. Licensee MDPI, Basel, Switzerland. This article is an open access article distributed under the terms and conditions of the Creative Commons Attribution (CC BY) license (<https://creativecommons.org/licenses/by/4.0/>).

1. Introduction

Recently, magnetic coupling technology based on the concept of magnetic induction (MI) has been widely used in eddy current testing (ECT) [1], MI-based communication [2], and wireless power transmission (WPT) due to its advantages of isolation and convenience [3–5]. Especially in the underwater environment, WPT technology can overcome the problem of rapid energy supply for autonomous underwater vehicles (AUVs) [6–9]. As a result, it is of great significance to develop a WPT system for underwater environments.

The WPT system used in underwater environments is similar to that used in air. It couples the alternating power generated by the primary side to the secondary side through a pair of coils, and the secondary side obtains direct current (DC) power through rectification. The difference is that the media between the coils is conductive water. Therefore, the magnetic coupling characteristics are different from that in air. It has been reported that the power transmission efficiency and capacity are related to the mutual coupling of the coils [10]. In the design process of WPT, most of the work is the design and optimization of the coils [11]. Thus, the mutual coupling analysis of the coils in water is an important topic for the design of the underwater WPT system.

It is usually necessary to carefully design the shape and installation position of the coils for the reliable coupling between coils in the power transmission system. There are inevitably magnetic materials and conductive materials around coils, which makes the coupling analysis between coils more complicated. However, the mutual impedance test is often carried out after the coils are processed. In order to estimate mutual impedance, numerous methods have been proposed by the researchers in order to calculate the mutual impedance of the coils. In [12], the magnetic vector potential approach is used to calculate the mutual inductance of two circular coils arbitrarily placed with respect to each other. This paper gives the mutual inductance calculation method of two coils in a non-conductive

environment based on the Neumann formula. In [13], the mutual impedance characteristics of two coils above a conducting plate are studied. The conducting plate will not only cause the change of the real part of the mutual impedance (the effect of the losses in the media), but also affect the imaginary part (mutual inductance). In [14], the influence of the conductivity of the medium on the mutual inductance is systematically studied. The research shows that the existence of the conductive medium will make the mutual inductance become complex. In [15], the mutual inductance between two planar coils is developed, and an analytical expression of the mutual inductance with respect to the properties of the media is carried out. However, this paper focuses on the influence of the material of the coil substrate on the mutual inductance of the coils. The influence of the medium between coils on mutual inductance has not been studied. In [16], an exponential attenuation factor is introduced to express the effect of conductive media on mutual impedance. The attenuation rate depends on the permeability, conductivity and dielectric constant of the media. However, in the MI region, the change of magnetic field is usually a complex function of the electrical parameters of the media and distance, so the introduction of exponential attenuation factor cannot well express the effect of the media on mutual impedance. In [17], the eddy current equivalent resistance is introduced to express the influence of water on the electrical parameters of the coil. However, when the coil is close to the conductive medium, it will not only cause the change of self inductance and AC resistance, but also form eddy currents in the conductive medium and produce ohmic loss. The eddy current equivalent resistance cannot directly express the influence of conductive medium on the coil coupling characteristics. In addition, a variety of measurement methods have been proposed to measure the mutual impedance of the coils and study the characteristics of media [18,19].

In this paper, the planar circular coil is taken as an example, and the mutual impedance of the coils immersed in water is analyzed from the perspective of magnetic vector potential by using the Truncated Region Eigenfunction Expansion (TREE) method [20,21]. The influence of truncation region and summation term on the accuracy of calculation results is analyzed. In addition, the influence of excitation frequency and the conductivity of media on mutual impedance is systematically studied, and the similarities and differences of mutual impedance in air and water are compared. The models can be used to analyze the coil coupling characteristics in the presence of conductive medium, which is helpful for the design process.

The organization of this paper is as follows. Section 2 introduces the mutual impedance model of coils immersed in water from the perspective of magnetic vector potential. In Section 3, the influence of truncation region and summation term on the accuracy of the proposed model is analyzed. In Section 4, an experiment is established to verify previous conclusions. Finally, the most important conclusions are summarized in Section 5.

2. Mutual Impedance of Two Coils of Filamentary Currents

The structure of the analyzed system is shown in Figure 1. In this figure, two coils insulated by small dielectric boxes are immersed in water. The two coils have n_i and n_j turns, respectively. In this approach, the multi-turn coil is modeled as a series of circular filamentary coil. The coil i is driven by a constant current I at angular frequency ω . The vertical distance of the two coils is d . The electromagnetic model of the coils depicted in Figure 1 is shown in Figure 2. Space is divided into six sections. The dielectric box is replaced by an infinitely wide dielectric layer. Region I, IV, and VI are characterized by electrical conductivity σ and magnetic permeability μ of water, and Region II, III, and V are characterized by $\sigma = 0$ and $\mu = 1$. With axial symmetry, the coil current density has only an azimuthal component; therefore, the vector potential becomes a scalar one. The potential A in all regions satisfies the following differential equation for the circular filamentary coil with radius r_0 and height z_0 .

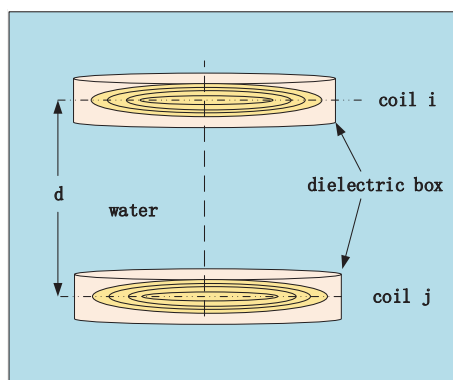


Figure 1. Schematic diagram of coils immersed in water.

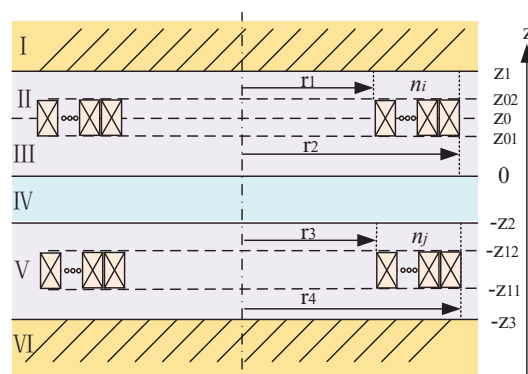


Figure 2. 2D axisymmetric view of the coils in the presence of water.

$$\frac{\partial^2 A}{\partial r^2} + \frac{1}{r} \frac{\partial A}{\partial r} - \frac{A}{r^2} + \frac{\partial^2 A}{\partial z^2} = k_i^2 A - \mu_0 \iota_0 \tag{1}$$

where ι_0 represents the current density of the circular filamentary coil, it can be described as

$$\iota_0 = I\delta(r - r_0)(z - z_0) \tag{2}$$

where $k_i^2 = j\omega\mu_r\mu_0\sigma_i$, the general form of the solution can be expressed as a series

$$A(r, z) = \sum_{i=1}^{\infty} [A_i J_1(\kappa_i r) + B_i Y_1(\kappa_i r)] [C_i e^{\lambda_i z} + D_i e^{-\lambda_i z}] \tag{3}$$

where $\lambda_i = \sqrt{\kappa_i^2 + j\omega\mu_r\mu_0\sigma_i}$, J_1 is the first-kind order-one Bessel function, and Y_1 is the second-kind order-one Bessel function. Because the electromagnetic field generated by the coil i does not extend to great distances, it can be assumed that potential vanishes at $r = h$, i.e., $A(h, z) = 0$. In particular, in Region I, $C_i^{(1)} = 0$, and in Region VI, $D_i^{(6)} = 0$ to ensure that the potential remains finite at $z = \pm\infty$. B_i should be 0 due to the divergence of $Y_1(0)$. Therefore the eigenvalues κ_i are the roots of the equation:

$$J_1(\kappa_i h) = 0 \tag{4}$$

Therefore, the components of the magnetic vector potential in all regions can be expressed as

$$\left\{ \begin{array}{l} A_1(r, z) = \sum_{i=1}^{\infty} J_1(\kappa_i r) e^{-\lambda_i z} D_i^{(1)} \\ A_2(r, z) = \sum_{i=1}^{\infty} J_1(\kappa_i r) (e^{\kappa_i z} C_i^{(2)} + e^{-\kappa_i z} D_i^{(2)}) \\ A_3(r, z) = \sum_{i=1}^{\infty} J_1(\kappa_i r) (e^{\kappa_i z} C_i^{(3)} + e^{-\kappa_i z} D_i^{(3)}) \\ A_4(r, z) = \sum_{i=1}^{\infty} J_1(\kappa_i r) (e^{\lambda_i z} C_i^{(4)} + e^{-\lambda_i z} D_i^{(4)}) \\ A_5(r, z) = \sum_{i=1}^{\infty} J_1(\kappa_i r) (e^{\kappa_i z} C_i^{(5)} + e^{-\kappa_i z} D_i^{(5)}) \\ A_6(r, z) = \sum_{i=1}^{\infty} J_1(\kappa_i r) e^{\lambda_i z} C_i^{(6)} \end{array} \right. \quad (5)$$

From the continuity of B_z and H_r at the five interfaces of the six layers, we get

$$\left\{ \begin{array}{l} A_1(r, z_1) = A_2(r, z_1) \\ \left. \frac{\partial A_1(r, z)}{\partial z} \right|_{z=z_1} - \left. \frac{\partial A_2(r, z)}{\partial z} \right|_{z=z_1} = 0 \\ A_2(r, z_0) = A_3(r, z_0) \\ \left. \frac{\partial A_2(r, z)}{\partial z} \right|_{z=z_0} - \left. \frac{\partial A_3(r, z)}{\partial z} \right|_{z=z_0} = -\mu_0 I_0 \\ A_3(r, 0) = A_4(r, 0) \\ \left. \frac{\partial A_3(r, z)}{\partial z} \right|_{z=0} - \left. \frac{\partial A_4(r, z)}{\partial z} \right|_{z=0} = 0 \\ A_4(r, -z_2) = A_5(r, -z_2) \\ \left. \frac{\partial A_4(r, z)}{\partial z} \right|_{z=-z_2} - \left. \frac{\partial A_5(r, z)}{\partial z} \right|_{z=-z_2} = 0 \\ A_5(r, -z_3) = A_6(r, -z_3) \\ \left. \frac{\partial A_5(r, z)}{\partial z} \right|_{z=-z_3} - \left. \frac{\partial A_6(r, z)}{\partial z} \right|_{z=-z_3} = 0 \end{array} \right. \quad (6)$$

Substituting (5) into the boundary conditions (6), there are

$$\left\{ \begin{aligned} \sum_{i=1}^{\infty} J_1(\kappa_i r) e^{-\lambda_i z_1} D_i^{(1)} &= \sum_{i=1}^{\infty} J_1(\kappa_i r) [e^{\kappa_i z_1} C_i^{(2)} + e^{-\kappa_i z_1} D_i^{(2)}] \\ \sum_{i=1}^{\infty} -J_1(\kappa_i r) \lambda_i e^{-\lambda_i z_1} D_i^{(1)} - \sum_{i=1}^{\infty} J_1(\kappa_i r) \kappa_i (e^{\kappa_i z_1} C_i^{(2)} - e^{-\kappa_i z_1} D_i^{(2)}) &= 0 \\ \sum_{i=1}^{\infty} J_1(\kappa_i r) (e^{z_0 \kappa_i} C_i^{(2)} + e^{-z_0 \kappa_i} D_i^{(2)}) &= \sum_{i=1}^{\infty} J_1(\kappa_i r) (e^{z_0 \kappa_i} C_i^{(3)} + e^{-z_0 \kappa_i} D_i^{(3)}) \\ \sum_{i=1}^{\infty} J_1(\kappa_i r) \kappa_i (e^{\kappa_i z_0} C_i^{(2)} - e^{-\kappa_i z_0} D_i^{(2)}) - \sum_{i=1}^{\infty} J_1(\kappa_i r) \kappa_i (e^{\kappa_i z_0} C_i^{(3)} - e^{-\kappa_i z_0} D_i^{(3)}) &= -\mu_0 t_0 \\ \sum_{i=1}^{\infty} J_1(\kappa_i r) (C_i^{(3)} + D_i^{(3)}) &= \sum_{i=1}^{\infty} J_1(\kappa_i r) (C_i^{(4)} + D_i^{(4)}) \\ \sum_{i=1}^{\infty} J_1(\kappa_i r) \kappa_i (C_i^{(3)} - D_i^{(3)}) - \sum_{i=1}^{\infty} J_1(\kappa_i r) \lambda_i (C_i^{(4)} - D_i^{(4)}) &= 0 \\ \sum_{i=1}^{\infty} J_1(\kappa_i r) (e^{-z_2 \lambda_i} C_i^{(4)} + e^{z_2 \lambda_i} D_i^{(4)}) &= \sum_{i=1}^{\infty} J_1(\kappa_i r) (e^{-z_2 \kappa_i} C_i^{(5)} + e^{z_2 \kappa_i} D_i^{(5)}) \\ \sum_{i=1}^{\infty} J_1(\kappa_i r) \lambda_i (e^{-z_2 \lambda_i} C_i^{(4)} - e^{z_2 \lambda_i} D_i^{(4)}) - \sum_{i=1}^{\infty} J_1(\kappa_i r) \kappa_i (e^{-z_2 \kappa_i} C_i^{(5)} - e^{z_2 \kappa_i} D_i^{(5)}) &= 0 \\ \sum_{i=1}^{\infty} J_1(\kappa_i r) (e^{-z_3 \kappa_i} C_i^{(5)} + e^{z_3 \kappa_i} D_i^{(5)}) &= \sum_{i=1}^{\infty} J_1(\kappa_i r) e^{-z_3 \lambda_i} C_i^{(6)} \\ \sum_{i=1}^{\infty} J_1(\kappa_i r) \kappa_i (e^{-z_3 \kappa_i} C_i^{(5)} - e^{z_3 \kappa_i} D_i^{(5)}) - \sum_{i=1}^{\infty} J_1(\kappa_i r) \lambda_i e^{-z_3 \lambda_i} C_i^{(6)} &= 0 \end{aligned} \right. \quad (7)$$

Multiply both sides of the above equations by $J_1(\kappa_i r) r$, integrate from 0 to h and use the orthogonality property of the Bessel function, we get

$$\left\{ \begin{aligned} e^{-\lambda_i z_1} D_i^{(1)} &= e^{\kappa_i z_1} C_i^{(2)} + e^{-\kappa_i z_1} D_i^{(2)} \\ -\lambda_i D_i^{(1)} e^{-\lambda_i z_1} - \kappa_i (C_i^{(2)} e^{\kappa_i z_1} - D_i^{(2)} e^{-\kappa_i z_1}) &= 0 \\ e^{\kappa_i z_0} C_i^{(2)} + e^{-\kappa_i z_0} D_i^{(2)} - e^{\kappa_i z_0} C_i^{(3)} - e^{-\kappa_i z_0} D_i^{(3)} &= 0 \\ \frac{[hJ_0(\kappa_i h)]^2}{2} [\kappa_i (e^{\kappa_i z_0} C_i^{(2)} - e^{-\kappa_i z_0} D_i^{(2)}) - \kappa_i (e^{\kappa_i z_0} C_i^{(3)} - e^{-\kappa_i z_0} D_i^{(3)})] &= -\mu_0 t_0 r_0 J_1(\kappa_i r_0) \\ C_i^{(3)} + D_i^{(3)} &= C_i^{(4)} + D_i^{(4)} \\ \kappa_i (C_i^{(3)} - D_i^{(3)}) &= \lambda_i (C_i^{(4)} - D_i^{(4)}) \\ C_i^{(4)} e^{-\lambda_i z_2} + D_i^{(4)} e^{\lambda_i z_2} - C_i^{(5)} e^{-\kappa_i z_2} - D_i^{(5)} e^{\kappa_i z_2} &= 0 \\ \lambda_i (C_i^{(4)} e^{-\lambda_i z_2} - D_i^{(4)} e^{\lambda_i z_2}) - \kappa_i (C_i^{(5)} e^{-\kappa_i z_2} - D_i^{(5)} e^{\kappa_i z_2}) &= 0 \\ C_i^{(5)} e^{-\kappa_i z_3} + D_i^{(5)} e^{\kappa_i z_3} - C_i^{(6)} e^{-\lambda_i z_3} &= 0 \\ \kappa_i (C_i^{(5)} e^{-\kappa_i z_3} - D_i^{(5)} e^{\kappa_i z_3}) - \lambda_i (C_i^{(6)} e^{-\lambda_i z_3}) &= 0 \end{aligned} \right. \quad (8)$$

Then we get the coefficients $C_i^{(5)}$, $D_i^{(5)}$ by solving (8).

$$\begin{aligned} C_i^{(5)} &= 4t_0 e^{-z_0 \kappa_i + 2z_3 \kappa_i + z_2(\kappa_i + \lambda_i)} r_0 \lambda_i (\kappa_i + \lambda_i) [e^{2z_0 \kappa_i} (\lambda_i - \kappa_i) - e^{2z_1 \kappa_i} (\kappa_i + \lambda_i)] \mu_0 J_1(\kappa_i r_0) / \\ &h^2 J_0^2(h\kappa_i) [-e^{2z_2(\kappa_i - \lambda_i)} - e^{2(z_1 + z_3)\kappa_i + 2z_2 \lambda_i} (\kappa_i + \lambda_i)^4 + e^{2z_2 \kappa_i} (\kappa_i^2 - \lambda_i^2)^2 - e^{2(z_1 + z_2)\kappa_i} (\kappa_i^2 - \lambda_i^2)^2 \\ &- e^{2z_3 \kappa_i} (\kappa_i^2 - \lambda_i^2)^2 + e^{2(z_1 + z_3)\kappa_i} (\kappa_i^2 - \lambda_i^2)^2 + e^{2z_3 \kappa_i + 2z_2 \lambda_i} (\kappa_i^2 - \lambda_i^2)^2 + e^{2z_1 \kappa_i + 2z_2(\kappa_i + \lambda_i)} (\kappa_i^2 - \lambda_i^2)] \quad (9) \\ D_i^{(5)} &= \frac{(\lambda_i - \kappa_i)}{(\lambda_i + \kappa_i)} e^{2z_3 \kappa_i} C_i^{(5)}(r_0, z_0) \end{aligned}$$

On the assumption that a multi-turn coil can be approximated by the superposition of a number of filamentary coils, and the coil has a rectangular cross-section. If the current density is constant over the dimensions of the coil, the equivalent current density of coil i can be expressed as follows

$$\iota = n_i I / [(r_2 - r_1)(z_{02} - z_{01})] \quad (10)$$

If we let the current distribution in the filamentary coils approach a continuous distribution, we can approximate the coil i of finite cross-section by the integral [20,21]. Replace the current density ι_0 in (9) with ι , we get

$$\begin{aligned} C_i^{(5)} &= \int_{r_1}^{r_2} \int_{z_{01}}^{z_{02}} C_i^{(5)}(r_0, z_0) dr_0 dz_0 \\ D_i^{(5)} &= \int_{r_1}^{r_2} \int_{z_{01}}^{z_{02}} D_i^{(5)}(r_0, z_0) dr_0 dz_0 \end{aligned} \quad (11)$$

According to the law of electromagnetic induction, the voltage induced in a length of wire can be expressed as

$$V = \oint_C E \cdot dl = -j\omega \oint_C A_5 \cdot dl \quad (12)$$

where dl is a vector differential line element tangential to the path of the source current. The total voltage induced in the coil j is then

$$V_{total} = \sum_{i=1}^{n_j} V_i \quad (13)$$

where V_i can be calculated by (12), then we can approximate the sum operation as an integral operation:

$$V_{total} = -j\omega N_D \iiint_{\Omega} A_5 dV \quad (14)$$

where $N_D = \frac{n_j}{(r_4 - r_3)(z_{11} - z_{12})}$ represents the turn density of the coil j . The mutual impedance Z_{ij} is defined as the ratio between V_{total} and the driving current I , as it can be seen as follows:

$$Z_{ij} = \frac{V_{total}}{I} = R_{ij} + j\omega M \quad (15)$$

The parameter R_{ij} represents the effect of the losses in the media, it represents a component of the induced voltage V_{total} in phase with the driving current I . The parameter M is the total mutual inductance between the two coils [15]. It can be seen from the above formula that in the presence of conductive media, mutual impedance becomes complex.

3. Convergence Analysis of the Model

In the analysis of the previous section, the mutual impedance is expressed in the form of series. Obviously, the results are closely related to the sum term N and truncation region h . The convergence of TREE method has been fully verified in the field of ECT [21]. Therefore, this section focuses on the influence of summation term N and truncation region h on the accuracy of calculation results in the presence of water, which can be used as a theoretical guide for engineering application.

The summation term N is considered as a variable that ranges from 1 to 40. The truncation region h is swept from $h = r_2$ to $h = 10r_2$. The distance between the two coils is equal to 2 cm. The outer radius and inner radius of the coils are 10 cm and 6 cm, respectively. The number of turns is 20, and the excitation frequency is fixed at 100 kHz. The conductivity of water is set to $\sigma = 4$ S/m. According to these conditions, the calculated results are shown in Figures 3 and 4. As it can be seen, different summation terms N and h can lead to different calculation results. For any h , the results will converge with the increase of the sum term N . Basically, when the sum term is greater than 20, the results will converge.

However, for different h , the convergence results are different. When h is equal to r_2 or $2r_2$, the results of convergence are quite different. However, when h is greater than $3r_2$, the final convergence result is almost the same. This indicates that the distribution region of magnetic field generated by excitation current is limited. Therefore, the hypothesis that the magnetic vector potential is equal to 0 when $r = h$ is reasonable. Thus, in practical engineering application, the truncation region can be selected according to the needs of calculation accuracy and calculation time.

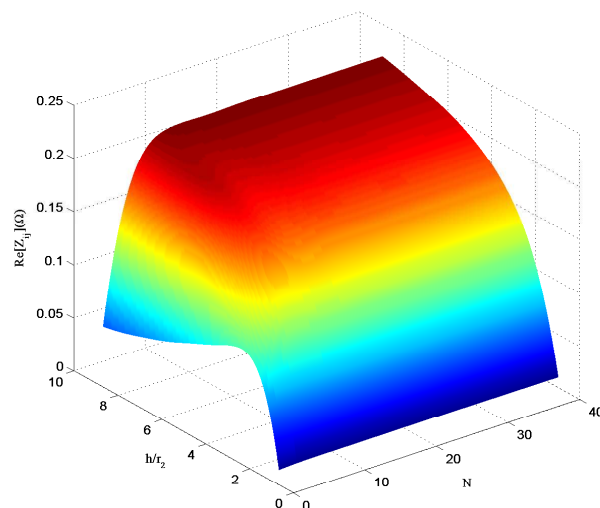


Figure 3. The influence of N and h on the real part of mutual impedance.

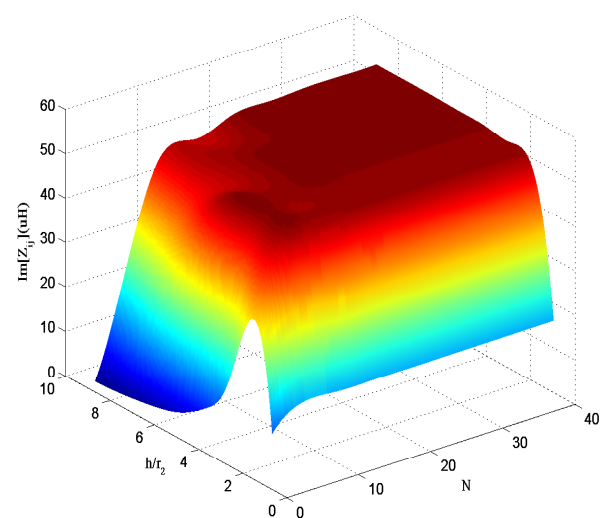


Figure 4. The influence of N and h on the imaginary part of mutual impedance.

4. Experimental Results and Discussion

An experimental is implemented to verify the theoretical and simulation results as shown in Figure 5. Two identical coils have been wound by copper wires with a diameter of 1 mm, and each one of them has 20 turns of external and internal radii of 100 mm and 60 mm, respectively. In order to prevent leakage of current, the two coils are insulated from the surrounding environment by small dielectric boxes made of acrylic material. The dielectric box size is 600 mm \times 800 mm \times 10 mm. In order to ensure the accuracy of the coil position during the test, coils are fixed on the inner surface of the dielectric boxes by glue. The dielectric boxes are immersed in a water tank with the size of 900 mm \times 800 mm \times 600 mm. The inner wall of the water tank is designed with a guide groove, which can be used for fixing the dielectric boxes. During the experiment, the conductivity of water is adjusted by adding sea salt into the water. Measurements

have been performed by using the Wayne Kerr 6500B Impedance Analyzer. The mutual impedance is measured by the in-phase and the opposing-phase connections of the two coils. Two different connections give the following impedances applying the reciprocity theorem [15]:

$$\begin{aligned} Z_i &= (R_i + R_j) + j\omega(L_i + L_j) + 2Z_{ij} \\ Z_o &= (R_i + R_j) + j\omega(L_i + L_j) - 2Z_{ij} \end{aligned} \quad (16)$$

where Z_{ij} is the mutual impedances between the two coils. R_i, R_j are the parasitic resistance of the coil i and coil j , while L_i, L_j are the self-inductances of the two coils.

Subtract the left side from the left side, and the right side from the right side of the above two equations, we get

$$Z_{ij} = \frac{Z_i - Z_o}{4} = R_{ij} + j\omega M \quad (17)$$

$$M = \text{Im}(Z_{ij})/\omega \quad (18)$$

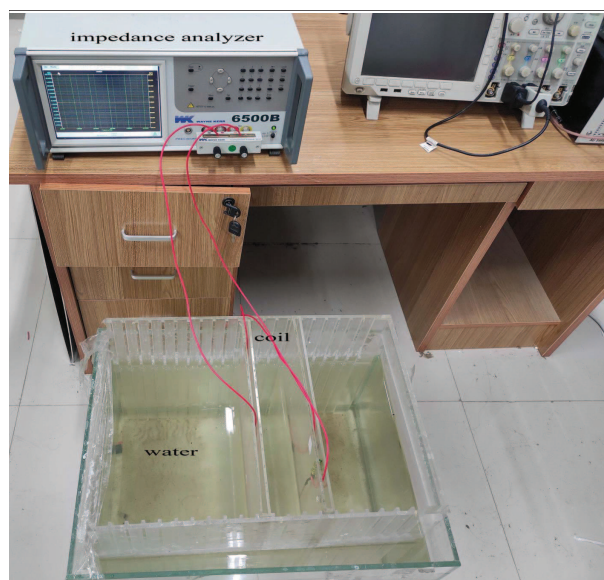


Figure 5. Image of the experimental setup.

The FEA tool COMSOL is used to model and compare the estimated results with the experimental results. The selected space dimension is 2D axisymmetric, the physical field is magnetic field. Two coaxial uniform multi-turn coils are constructed, and the number of turns is 20. The coils are surrounded by a rectangular region with width of 40 cm and height of 1 cm, respectively. The region is defined as air. The regions are surrounded by a rectangular region with width of 80 cm and height of 30 cm. The models of the coils immersed in air or water can be constructed by modifying the material properties of this area to water or air. The element size of mesh is normal. By applying 1A excitation current to one coil and setting the other coil as open circuit, the mutual impedance between coils is obtained by measuring the voltage at both ends of the open circuit coil.

4.1. Influence of the Conductivity in the Mutual Impedance

In order to investigate the effect of the conductivity in the mutual impedance, the coils in air and immersed in water with different conductivity are both tested in this experiment. As depicted in Figure 5, the coils are parallel and coaxial in the water tank. When the water tank is not filled with water, the mutual impedance between the coils in air is tested, and different conductivity is generated by adding sea salt into the water tank. The experimental results are shown in Figure 6a,b compared with the analytical results. According to the

influence of summation term N and truncation region h on the accuracy of calculation results in the previous section, $N = 30$, and $h = 5r_2$ are selected in this case. The distance between the two coils is 20 mm, and the measurement frequency is fixed at 100 kHz. The conductivity ranges from $\sigma = 0$ S/m, which corresponds to the air, to $\sigma = 4$ S/m, which corresponds to seawater. It is obviously observed that the estimated results have the same trend with the simulation and measurement results. As shown in Figure 6a, the real part of mutual impedance increases with the increase of conductivity. When the conductivity is zero, the difference between the estimated results and the simulation and measured results is large. The estimated real part of mutual impedance is zero. When the conductivity increases, the difference between the estimated results and the simulation and measured results is gradually narrowed. This is because the proposed model assumes that the current in the coil is uniformly distributed and does not consider skin effect and proximity effect. However, the actual coil inevitably has the above two effects. There is a coupling between the turns of the coil due to the proximity effect. At the same time, the magnetic field generated by the eddy current in water will also affect coupling between the coils. When the medium conductivity σ is zero, the real part of mutual impedance mainly comes from the influence of proximity effect, which is not considered in the model. When σ increases gradually, the magnetic field produced by eddy current in water is the main reason for the change of the real part of mutual impedance. Therefore, when the conductivity is low, the real part estimation error is larger, while the error decreases when the conductivity increases gradually. In Figure 6b, there is only a slight reduction in the imaginary part of mutual impedance, when $\sigma = 0$ S/m, the imaginary part is equal to 51.56 μH , and when $\sigma = 4$ S/m, the imaginary part is reduced to 51.52 μH . The estimated error is about 4%. The estimation error of imaginary part mainly comes from the definition of equivalent turn density of coil j . In order to simplify the calculation, the cross-section of coil area is assumed to be a rectangle, and the equivalent turn density is used to approximate the coil space. However, the cross-section of each turn of the actual and simulated coils is circular, and the coil does not occupy the whole rectangular section space. Thus, there is a constant bias in the estimation. The change of mutual impedance with conductivity shows that in the case of medium conductivity and excitation frequency of the coil are not too high, the additional magnetic field induced by eddy current in the medium has little effect on the original magnetic field generated by the excitation coil, so the mutual inductance in the water is almost the same as that in air.

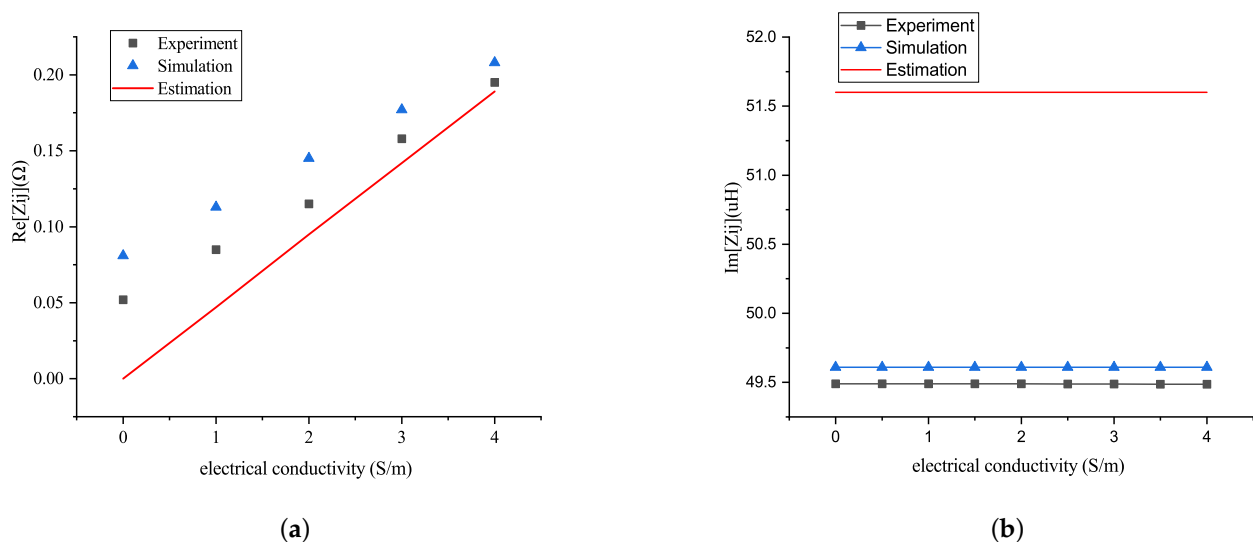


Figure 6. (a) The real part of mutual impedance of two coils as a function of the conductivity of media. (b) The imaginary part of mutual impedance of two coils as a function of the conductivity of media.

4.2. Influence of Frequency in the Mutual Impedance

In this case, the effects of excitation frequency in the mutual impedance are investigated. Considering that the change of the imaginary part is not obvious when the conductivity is less than 4 S/m, and in underwater environment, high frequency will cause high ohmic losses, this section focuses on the variation of mutual impedance with respect to frequency within 1 MHz when the coil is immersed in seawater. $N = 30$, and $h = 5r_2$ are also selected as in the previous section. As shown in Figure 7a,b, the results show that the imaginary part decreases with the increase of frequency, but the real part of mutual impedance increases with the increase of frequency. However, the imaginary part at tens of kHz and hundreds of kHz is only reduced a little, the real part of mutual impedance increases exponentially. With the increase of the coil excitation frequency, the estimation error of the real part increases gradually. With the increase of the excitation frequency of the coil, on the one hand, the eddy current energy in the water is enhanced. At the same time, due to the existence of skin effect and proximity effect, the current distribution in the coil can no longer be equivalent to uniform distribution. Therefore, the real part estimation error increases with the excitation frequency. It is precisely because the increase of frequency will cause the increase of energy loss in the medium, so the working frequency of underwater wireless power transmission system is usually around 200 kHz [6]. The estimated results of the model in this frequency band can be used for parameter optimization in the design phase.

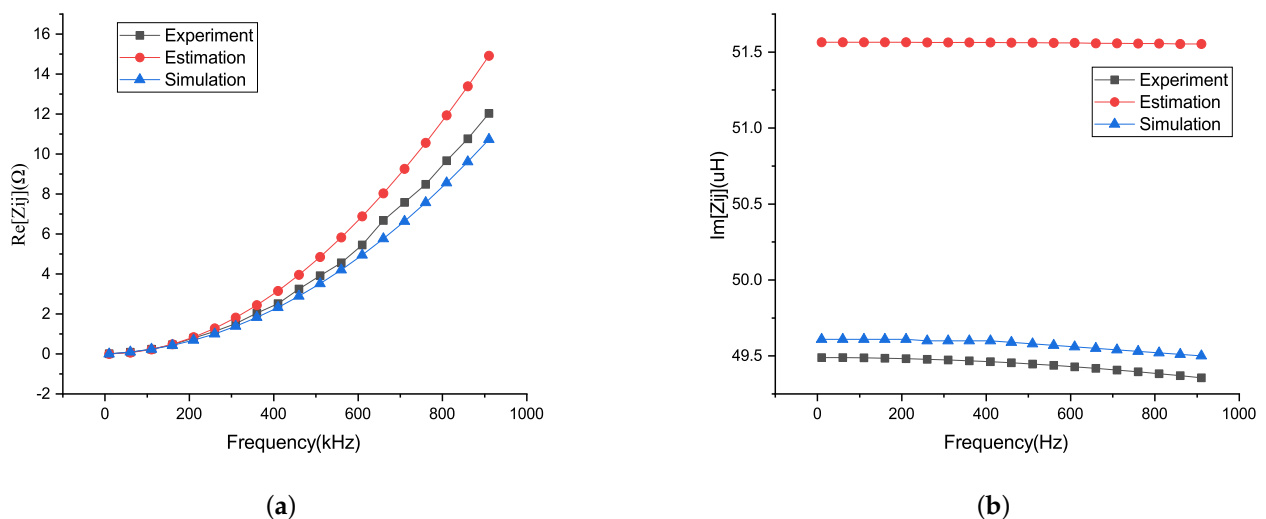


Figure 7. (a) The real part of mutual impedance of two coils as a function of the excitation frequency. (b) The imaginary part of mutual impedance of two coils as a function of the excitation frequency.

4.3. Variation of Mutual Impedance with Axial Displacement

In the underwater MI communication or WPT system, in order to ensure sufficient coupling between the coils, it is usually necessary to keep the coils coaxial. In this configuration, we focus on the influence of the axial displacement in the mutual impedance when the coil is immersed in water. In order to compare the effect of water on the mutual impedance, we also compare and test the mutual impedance in air. The measurement frequency is fixed at 100 kHz. The axial displacement is varied from $0.2r$ to $1.2r$. As shown in Figure 8a,b, when the axial displacement of the coil increases, both the real part and the imaginary part of mutual impedance decrease gradually. When the displacement increases to r , then the imaginary part decreases by about 0.8. It is worth mentioning that when the coil is in water and air, the trend of the imaginary part with axial displacement is almost the same.

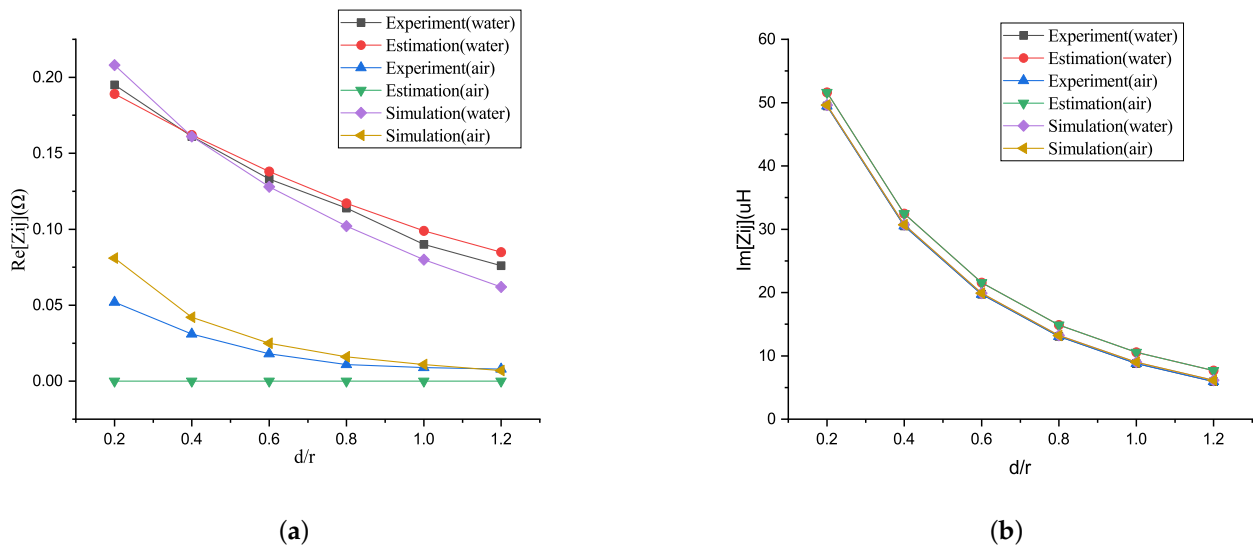


Figure 8. (a) The real part of mutual impedance of two coils with respect to axial displacement when $f = 100$ kHz, $\sigma = 0$ S/m, 4 S/m. (b) The imaginary part of mutual impedance of two coils with respect to axial displacement when $f = 100$ kHz, $\sigma = 0$ S/m, 4 S/m.

Because the frequency is also one of the factors that affect the mutual impedance between coils, the mutual impedance of coils with axial displacement at 10 kHz and 910 kHz is compared and tested when $\sigma = 4$ S/m. The results are shown in Figure 9a,b. It can be seen that Figure 9b, and Figure 8b are almost the same. This is because when the conductivity of the media is fixed, although the frequency has an impact on the imaginary part, the attenuation of the imaginary part is very small in the frequency range of interest. The difference is that the difference of excitation frequency will lead to the difference of the real part of mutual impedance.

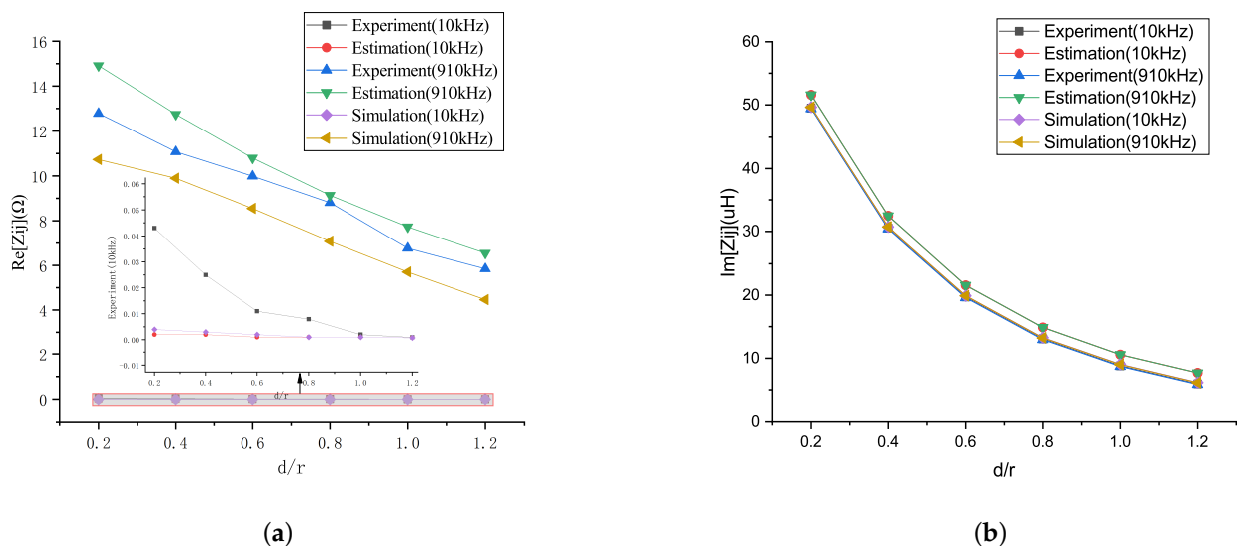


Figure 9. (a) The real part of mutual impedance of two coils with respect to axial displacement when $\sigma = 4$ S/m, $f = 10$ kHz, 910 kHz. (b) The imaginary part of mutual impedance of two coils with respect to axial displacement when $\sigma = 4$ S/m, $f = 10$ kHz, 910 kHz.

4.4. Error Analysis Introduced by the Assumption of Cross-Section

In the previous sections, we systematically analyzed the effects of medium conductivity, coil excitation frequency and axial displacement on mutual impedance. It can be seen that the method proposed in this paper can estimate the influence law of the above factors on the mutual impedance, but the estimation results will also have a small deviation.

Because the method proposed in this paper assumes that the current is evenly distributed in the coil, and for the convenience of calculation, the cross-section of the coil is approximated by a rectangular cross-section. Since the estimation error caused by current distribution has been analyzed in Sections 4.1 and 4.2, this section focuses on the error introduced by the assumption of the coil cross-section. Some calculations of the mutual impedance of the coils have been performed considering the number of turns as a parameter. The two coils are placed coaxial, the vertical distance is 2 cm, the inner radius of the coil remains unchanged, both are fixed at 6 cm, the excitation frequency is fixed at 100 kHz, and the conductivity of the medium is equal to 4 S/m. The number of turns has been swept from 10 to 20. In order to analyze the error of the model, both the circular cross-section closer to the real object and the rectangular cross-section used for approximate calculation are compared. The results are shown in Figure 10a,b. With the increase of the number of turns, the real and imaginary parts of mutual impedance increase gradually. This is because the increase of the number of turns increases the coupling area of the coil, but also increases the eddy current loss in water, which leads to the increase of the real and imaginary parts of mutual impedance. It can be seen from the simulation results that when the excitation frequency and other parameters remain unchanged, the simulation result with rectangular cross-section will make the estimation of the real part of mutual impedance smaller and the estimation result of the imaginary part of mutual impedance larger than that of circular cross-section. This also indirectly verifies the deviation of the method proposed in this paper. Therefore, in the process of solution, the rectangular cross-section can be used to approximate the cross-section of the coil, because the error caused by the assumption of rectangular cross-section is not large.

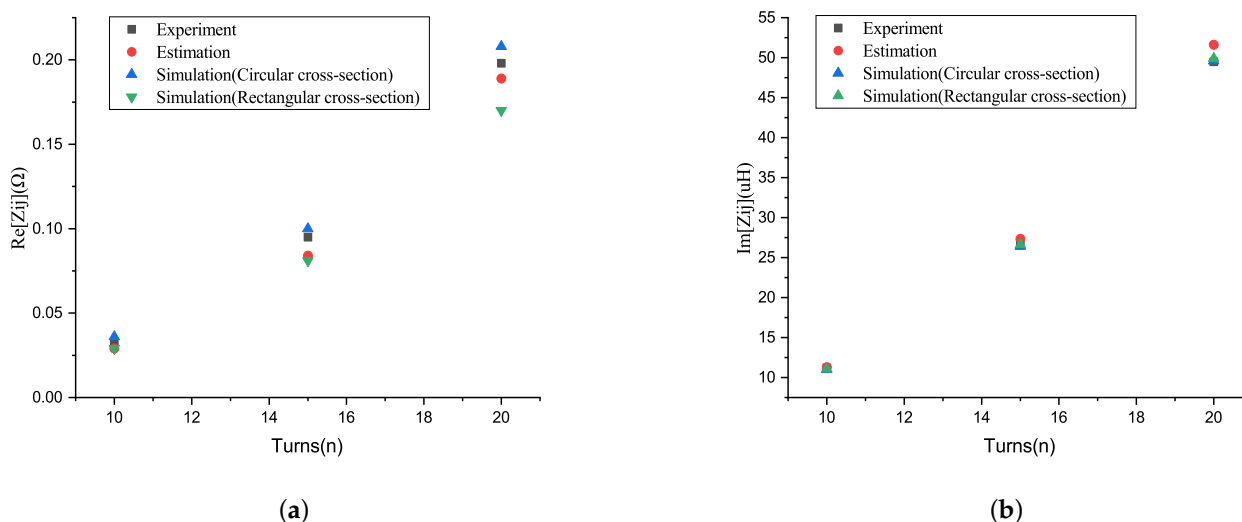


Figure 10. (a) The real part of mutual impedance of two coils with respect to the number of turns. (b) The imaginary part of mutual impedance of two coils with respect to the number of turns.

4.5. Discussion

In the design process of MI communication and WPT system, the most important work is the design of coil and the optimization of system parameters. The size of the coil and the operating frequency of the system are related to the communication distance of the MI communication system or the theoretical power capacity that can be transferred and power transmission efficiency of the WPT system. The model and calculation method proposed in this paper can be used to estimate the coupling state of coils in the design process. Through the estimation of the coupling state, combined with the electrical parameters of the coil itself, the working parameters of the system can also be optimized. Although the proposed model only studies the mutual impedance characteristics of the coil immersed in water, it can also be used in other cases where there is conductive medium. The coupling state of

the coil in the corresponding environment can be obtained simply by adding the dielectric layer and modifying the electrical parameters of each layer.

5. Conclusions

In this paper, a model of the mutual impedance between the coils immersed in water is established. In this model, the TREE method is adopted, and the magnetic vector potential is expressed as a series according to the continuity of magnetic induction intensity and magnetic field intensity at the media boundary. Finally, the expression of mutual impedance is derived. The calculated results are in good agreement with the experimental results in the frequency bands commonly used in underwater wireless power transmission system. The study shows that the mutual impedance between the coils is related to the excitation frequency and the conductivity of the media in the presence of water. The increase of frequency will cause the decrease of the imaginary part of mutual impedance, but compared with that in the air, it is only reduced by less than 1%. However, the real part of the mutual impedance increases significantly with the increase of frequency and conductivity. Therefore, resistive loss is the significant difference between coils in water and air.

Author Contributions: Conceptualization, P.L. and T.G.; methodology, P.L., Z.M.; software, P.L.; validation, P.L.; formal analysis, P.L., T.G., Z.M.; investigation, P.L.; resources, P.L.; data curation, P.L.; writing—original draft, P.L.; writing—review and editing, P.L., Z.M. and T.G.; visualization, P.L.; supervision, Z.M. and T.G.; project administration, Z.M. and T.G.; funding acquisition, Z.M. All authors have read and agreed to the published version of the manuscript.

Funding: This research was funded by the National Natural Science Foundation of China, grant number 61572404.

Institutional Review Board Statement: Not applicable.

Informed Consent Statement: Not applicable.

Data Availability Statement: Not applicable.

Conflicts of Interest: The authors declare no conflict of interest.

References

1. Miorelli, R.; Reboud, C.; Theodoulidis, T.P.; Poulakis, N.; Lesselier, D. Efficient modeling of ECT signals for realistic cracks in layered half-space. *IEEE Trans. Magn.* **2013**, *49*, 2886–2992. [[CrossRef](#)]
2. Tan, X.; Sun, Z.; Akyildiz, I.F. Wireless Underground Sensor Networks: MI-based communication systems for underground applications. *IEEE Antennas Propag. Mag.* **2015**, *57*, 74–87. [[CrossRef](#)]
3. Zhang, Z.; Pang, H.; Georgiadis, A.; Cecati, C. Wireless Power Transfer—An Overview. *IEEE Trans. Ind. Electron.* **2019**, *66*, 1044–1058. [[CrossRef](#)]
4. Kiani, M.; Jow, U.M.; Ghovanloo, M. Design and Optimization of a 3-Coil Inductive Link for Efficient Wireless Power Transmission. *IEEE Trans. Biomed. Circuits Syst.* **2011**, *5*, 579–591. [[CrossRef](#)] [[PubMed](#)]
5. Zhang, X.; Yuan, Z.; Yang, Q.; Li, Y.; Zhu, J.; Li, Y. Coil Design and Efficiency Analysis for Dynamic Wireless Charging System for Electric Vehicles. *IEEE Trans. Magn.* **2016**, *52*, 1. [[CrossRef](#)]
6. Yan, Z.; Zhang, Y.; Kan, T.; Lu, F.; Zhang, K.; Song, B.; Mi, C.C. Frequency Optimization of a Loosely Coupled Underwater Wireless Power Transfer System Considering Eddy Current Loss. *IEEE Trans. Power Electron.* **2019**, *66*, 3468–3476. [[CrossRef](#)]
7. Kan, T.; Mai, R.; Mercier, P.P.; Mi, C.C. Design and Analysis of a Three-Phase Wireless Charging System for Lightweight Autonomous Underwater Vehicles. *IEEE Trans. Power Electron.* **2018**, *33*, 6622–6632. [[CrossRef](#)]
8. McGinnis, T.; Henze, C.P.; Conroy, K. Inductive power system for autonomous underwater vehicles. *OCEANS* **2007**, *2007*, 1–5.
9. Zhou, J.; Li, D.J.; Chen, Y. Frequency selection of an inductive contactless power transmission system for ocean observing. *Ocean Eng.* **2018**, *60*, 175–185. [[CrossRef](#)]
10. Zhong, W.; Hui, S.Y.R. Maximum Energy Efficiency Operation of Series-Series Resonant Wireless Power Transfer Systems Using On-Off Keying Modulation. *IEEE Trans. Power Electron.* **2018**, *33*, 3595–3603. [[CrossRef](#)]
11. Kim, J.; Kim, J.; Kong, S.; Kim, H.; Suh, I.S.; Suh, N.P.; Cho, D.H.; Kim, J.; Ahn, S. Coil Design and Shielding Methods for a Magnetic Resonant Wireless Power Transfer System. *Proc. IEEE* **2013**, *101*, 1332–1342. [[CrossRef](#)]
12. Babic, S.; Sirois, F.; Akyel, C.; Girardi, C. Mutual Inductance Calculation Between Circular Filaments Arbitrarily Positioned in Space: Alternative to Grover’s Formula. *IEEE Trans. Magn.* **2010**, *46*, 3591–3600. [[CrossRef](#)]

13. Burke, S.K.; Ibrahim, M.E. Mutual impedance of air-cored coils above a conducting plate. *J. Phys. D Appl. Phys.* **2004**, *37*, 1857–1868. [[CrossRef](#)]
14. Vallecchi, A.; Chu, S.; Solymar, L.; Stevens, C.J.; Shamonina, E. Coupling between coils in the presence of conducting medium. *IET Microwaves Antennas Propag.* **2019**, *13*, 55–62. [[CrossRef](#)]
15. Acero, J.; Carretero, C.; Lope, I.; Alonso, R.; Burdio, J.M. Analysis of the Mutual Inductance of Planar-Lumped Inductive Power Transfer Systems. *IEEE Trans. Ind. Electron.* **2013**, *60*, 410–420. [[CrossRef](#)]
16. Ma, J.; Zhang, X.; Huang, Q.; Cheng, L.; Lu, M. Experimental Study on the Impact of Soil Conductivity on Underground Magneto-Inductive Channel. *IEEE Antennas Wirel. Propag. Lett.* **2015**, *14*, 1782–1785. [[CrossRef](#)]
17. Yan, Z.; Song, B.; Zhang, K.; Wen, H.; Mao, Z.; Hu, Y. Eddy current loss analysis of underwater wireless power transfer systems with misalignments. *J. Appl. Phys.* **2018**, *8*, 101421. [[CrossRef](#)]
18. Schaubert, M.J.; Newman, S.A.; Goodman, L.R.; Suzuki, I.S.; Suzuki, M. Measurement of mutual inductance from frequency dependence of impedance of AC coupled circuit using digital dual-phase lock-in amplifier. *Am. J. Phys.* **2008**, *76*, 129. [[CrossRef](#)]
19. Jash, A.; Roy, N.; Bag, B.; Banerjee, S.S. A two-coil mutual inductance technique to study the conductivity of metal and measurement of the superconducting transient temperature. *AIP Conf. Proc.* **2018**, *1942*, 060026.
20. Theodoulidis, T.P.; Kriezis, E.E. Series expansions in eddy current nondestructive evaluation. *J. Mater. Process. Technol.* **2005**, *161*, 343–347. [[CrossRef](#)]
21. Theodoulidis, T.P.; Bowler, J.R. The truncated region eigenfunction expansion method for the solution of boundary value problems in eddy current nondestructive evaluation. *Rev. Prog. Quant. Nondestruct. Eval.* **2004**, *24*, 403–408.